Heavy Vehicles on Minor Highway Bridges

stochastic modelling of surface irregularities

Nielsen, Søren R. K.; Kirkegaard, Poul Henning; Enevoldsen, I.

Publication date:
1997

Document Version
Publisher's PDF, also known as Version of record

INSTITUTTET FOR BYGNINGSTEKNIK
DEPT. OF BUILDING TECHNOLOGY AND STRUCTURAL ENGINEERING
AALBORG UNIVERSITET • AAU • AALBORG • DANMARK

STRUCTURAL RELIABILITY THEORY
PAPER NO. 170

S.R.K. NIELSEN, P.H. KIRKEGAARD, I. ENEVOLDSEN
HEAVY VEHICLES ON MINOR HIGHWAY BRIDGES - STOCHASTIC MODELLING OF SURFACE IRREGULATIRIES

AUGUST 1997 ISSN 1395-7953 R9720

The STRUCTURAL RELIABILITY THEORY papers are issued for early dissemination of research results from the Structural Reliability Group at the Department of Building Technology and Structural Engineering, University of Aalborg. These papers are generally submitted to scientific meetings, conferences or journals and should therefore not be widely distributed. Whenever possible reference should be given to the final publications (proceedings, journals, etc.) and not to the Structural Reliability Theory papers.

Printed at Aalborg University

INSTITUTTET FOR BYGNINGSTEKNIK
DEPT. OF BUILDING TECHNOLOGY AND STRUCTURAL ENGINEERING
AALBORG UNIVERSITET • AAU • AALBORG • DANMARK

STRUCTURAL RELIABILITY THEORY
PAPER NO. 170

S.R.K. NIELSEN, P.H. KIRKEGAARD, I. ENEVOLDSEN
HEAVY VEHICLES ON MINOR HIGHWAY BRIDGES - STOCHASTIC MODELLING OF SURFACE IRREGULATIRIES
AUGUST 1997 ISSN 1395-7953 R9720

ABSTRACT

The present paper worked out as a part of a research project on "Dynamic amplification factor of vehicle loadings on smaller bridges" establishes a two-dimensional spectral description of the road roughness surface based on measurements from a Danish road using a so-called Profilograph used by the Danish Road Directorate (Schmidt et al. 1996). The stochastic model for the surface irregularities models, based on the observations from the measured data, the deterministic trends in transversal (wheel tracking) as well as longitudinal direction (some long-waved tendency). Further, the bumps/expansion joints at the approaches to the bridge and the stochastic nature of the surface roughness are included into the model.

1. INTRODUCTION

The determination of the dynamic response of a bridge resulting from the passage of a vehicle across the span is a problem of great interest which can be seen from the literature reviews given in (Kirkegaard et al. 1997; Paultres et al. 1994) . The forces that produce the stresses in a bridge under dynamic loading are a result of the dead load of the vehicle and the bridge and the vehicle -bridge interactive forces. The forces depend on many factors such as the natural frequencies and damping ratios of the vehicle and bridge, the vehicle suspension system, speed of vehicle, the traffic intensity and the road surface irregularities of the bridge deck, see e.g. (Green et al. 1996; Inbanathan et al. 1988). Road surface irregularities are generally measured by one of the following two methods, i.e, 1) by using a profilometer; or 2) by calculating the road surface roughness backwards from vibrational data of the well-researched dynamic properties of the vehicle. Road surface irregularities have been measured in studies on the maintenance and repair of road surfaces and on riding comfort of vehicles , see e.g. (Dodds et al. 1973; Honda et al. 1983, Marcondes 1992). It has been found that most pavement profiles have very similar power spectral densities and that a single parameter known as the roughness index shifts the power density levels up and down, depending on the overall level of roughness. Further, by plotting the spectral densities versus the wave number in a double-logarithmic scale, it becomes obvious that all kinds of road pavements can be characterized by similar functions. This function may be approximated sufficiently by a straight line (Mathieu et al. 1991). Road surface roughness on bridges have been measured only rarely. Therefore, most studies done on the dynamic behaviour of bridges have used the spectral densities, which have been found for road surface roughness. In the paper (Honda et al. 1982) the spectral densities of road surface roughness on bridges have been found to be modelled in the same manner as the spectrum of surface roughness on general roads. However, all the proposed spectral densities of road surface roughness are only one-dimensional, i.e. the spectral densities model only road profile in longitudinal direction of the road and not in the transverse direction.

The present paper worked out as a part of a research project on "Dynamic amplification factor of vehicle loadings on smaller bridges" establishes a two-dimensional spectral description of the road roughness surface based on measurements from a Danish road using a so-called Profilograph used by the Danish Road Directorate (Schmidt et al. 1996). A part of the measured road includes a part of a bridge wherefore the irregularities due to the abutments also have been taken into the stochastic description of the road. The paper is organized in the following sections. Section 2 gives a description of the Profilograph and the data set considered. Next, in section 3 a model of a two-dimensional spectral density function of road surface roughness is given. Section 3, also deals with simulation of road surface profiles based on the two-dimensional spectral density function. Finally, in section 4 and 5 conclusions and references are given.

2. LASER-BASED MEASUREMENTS OF ROAD SURFACES

The measurements of the road irregularities considered in this paper have been obtained using a Profilograph. The following descriptions of the Profilograph is adapted from (Schmidt et al. 1996).

2.1 Description of the Profilograph used by the Danish Road Directorate

In 1991 the Danish Road Directorate introduced profilometric measurements of pavement surfaces by purchasing its first Profilograph. The concept of the Profilograph, see figure 2.1, is a system with several lasers positioned on a vertical adjustable beam in front of a vehicle, measuring a point on the pavement surface at every 5 mm in the longitudinal direction. The pavement's transverse profile is measured in points according to the lasers position on the beam covering a maximum width of 2.9 meters. In 1992, the Danish Road Directorate bought its second Profilograph and based on the experiences from the first device, the maximum measuring width was increased to 3.5 meters. The purpose of mounting the lasers on an adjustable beam is to assure that the measurements are performed within the lasers' measuring range and as close to the optimum measuring distance as possible. The position of the lasers on the beam takes into account that the shape of the pavement can be very different from a true plane in the wheel path. Therefore, in order to accurately determine possible rutting from a well-defined transverse profile of the pavement, the lasers are positioned closer to each other where rutting can be expected to occur. The profilographs are able to measure evenness in the speed of 5 to 130 km/h.

Figure 2.1 *Profilograph used by the Danish Road Directorate*

2.2 Presentation of the Measured Raw Data

A data series obtained by the Profilograph with a measuring width at 3.2 meters has been provided by the Danish Road Directorate. This means that the distance between the 25 lasers is as shown in figure 2.2. Laser no. 1 and no. 2 measure in the left and the right side of the road, respectively.

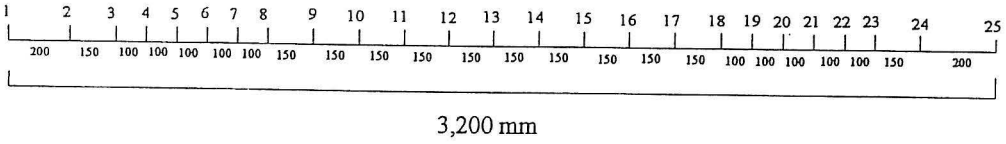

Figure 2.2 *Laser position for Profilograph*

The data series are measured in the left side of the road Åsvej in the municipality of Roskilde on the island Zealand. From the stationing km 15.872 (record no. 7722) to stationing km 15.672 (record no. 9692) with 0.1 m between each record number., i.e. a road with a length of 200 m has been measured. The middle of the bridge no. 138-009 (Åsvej) has stationing km 15.772. Figure 2.3 shows the measured road profile. In the longitudinal direction estimates of the road irregularities are given for each 0.1 m while in the transverse direction estimates are given corresponding to the laser positions shown in figure 2.2. Figure 2.4 shows the measured road profile after the mean values for each laser in longitudinal direction have been removed. It is seen that the measured road profile has large overall variations in the profiles together with the overall roughness. Figure 2.5 shows the measured road profile after these trends have been removed in the transversal direction. A typical wheel tracking pattern is seen. Next in figure 2.6 the Power Spectral Density (PSD) is shown versus the wave number in a double-logarithmic scale. It becomes obvious that the road irregularities can be approximated sufficiently by a straight line in this double-logarithmic scale. In order to see the variation of the PSD in the direction of the laser locations a straight line given by

$$\ln s_Y(k) = a\ln(k) + b \qquad (1)$$

has been fitted to the PSD for each laser. $s_Y(k)$ signifies the one-sided one-dimensional auto-spectrum only defined for positive (physical) wave-numbers. This quantity is thoroughly defined below in section 3. In double logarithmic mapping the spectrum is assumed linear with parameteres a, b and wave-numbers k, respectively. Figure 2.7 shows the results obtained by linear regression line using equation (1) to the PSD for each laser. Figure 2.8 shows the variation in the parameters a and b. The variation in the slope indicates that the road is smoother in the wheel tracking.

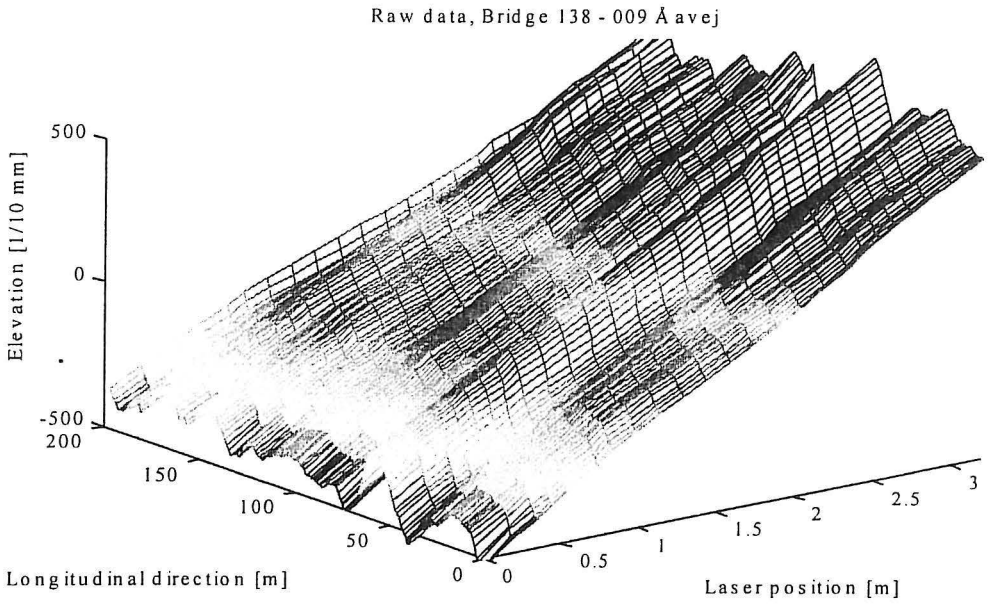

Figure 2.3 *The measured road profile from bridge 138 -009 (Åsvej). Laser no 1 in the left side of the road, laser no. 25 in the right side of the road.*

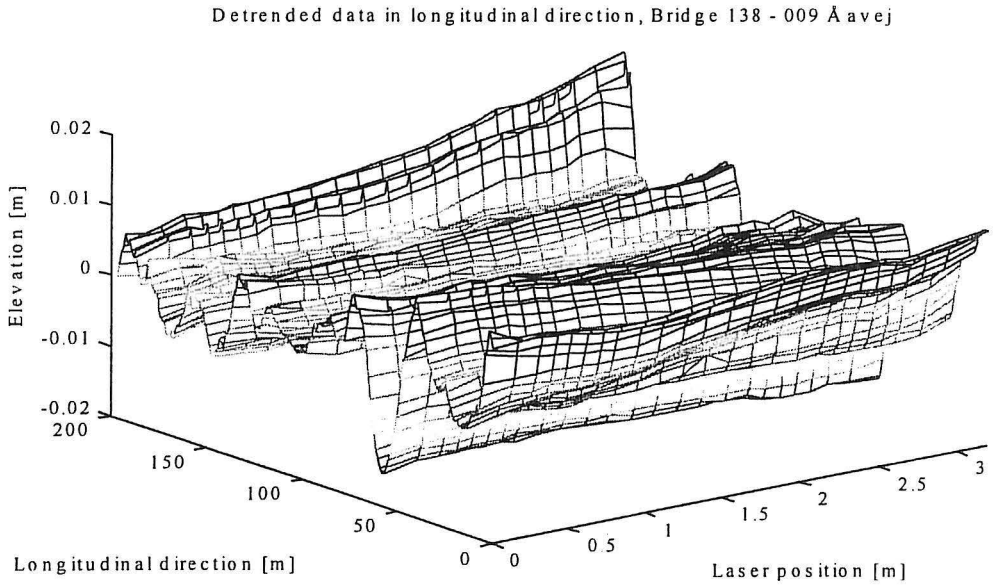

Figure 2.4 *The measured road profile from bridge 138 -009 (Åsvej). Laser no 1 in the left side of the road, laser no. 25 in the right side of the road. Mean removed in longitudinal direction*

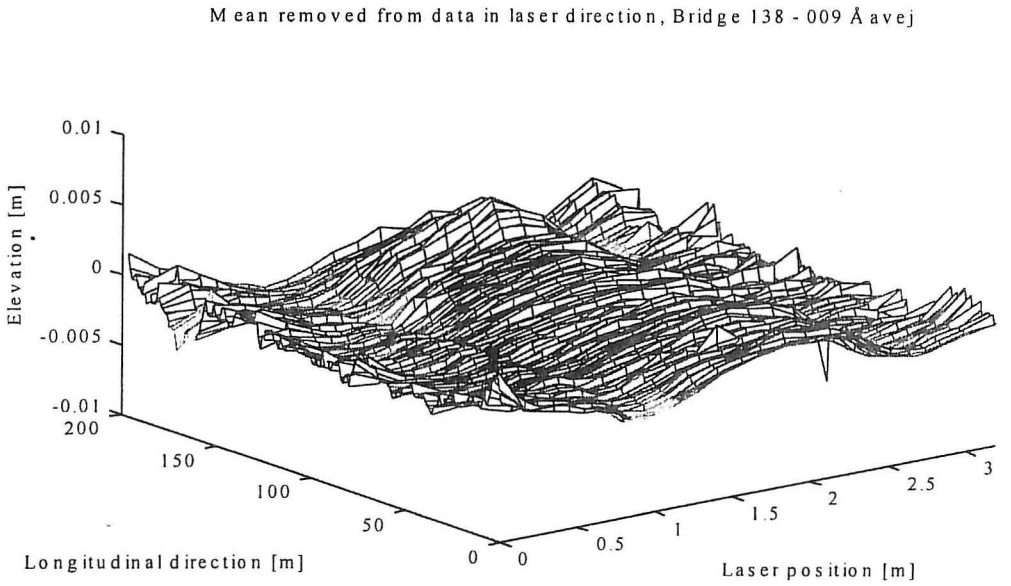

Figure 2.5 *The measured road profile from bridge 138 -009 (Åsvej). Laser no 1 in left side of the road, laser no. 25 in the right side of the road. Mean removed in laser direction*

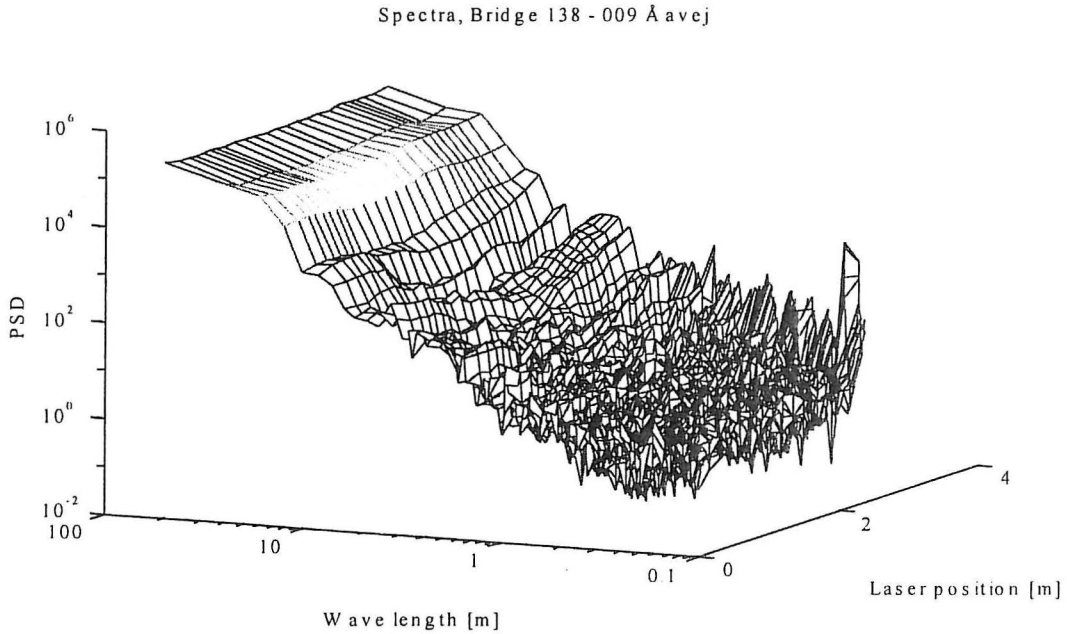

Figure 2.6 *PSD of the measured road profile from bridge 138 -009 (Åsvej) shown as a function of laser position and wave number in a double logarithmic mapping.*

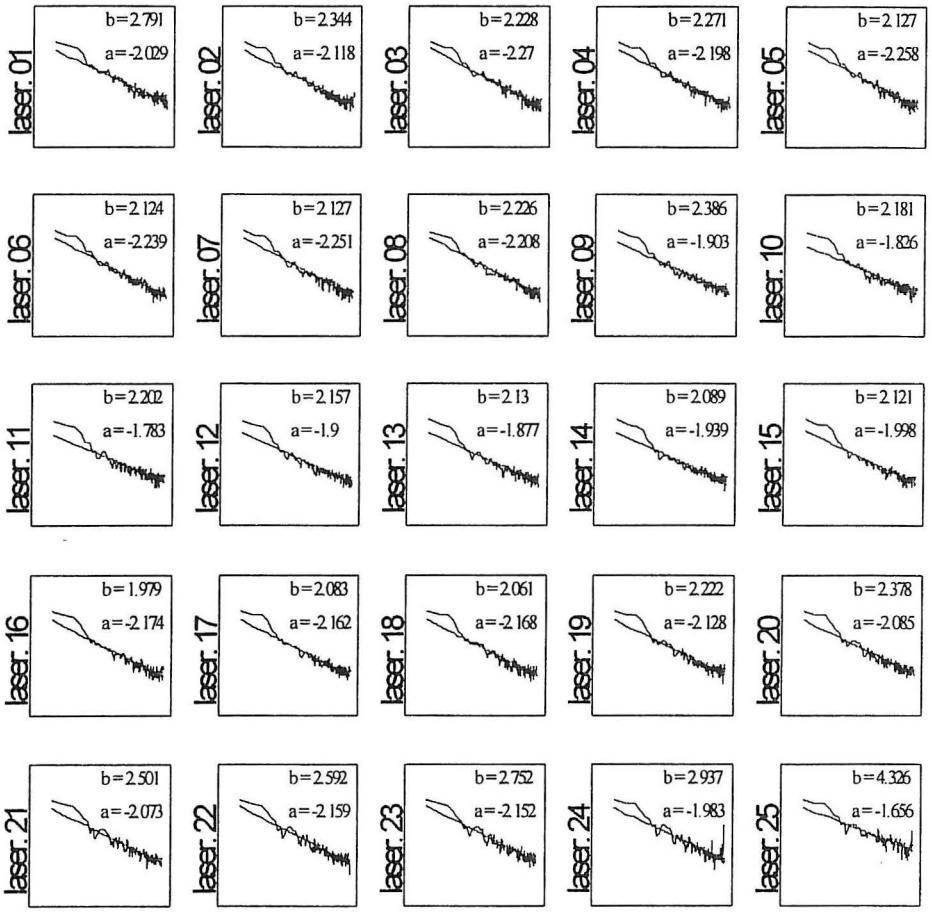

Figure 2.7 *PSD* $s_Y(k)$ *of the measured road profile from bridge 138 -009 (Åsvej) shown for each laser position and wave number in a double logarithmic mapping together with a linear regression line given by equation (1).*

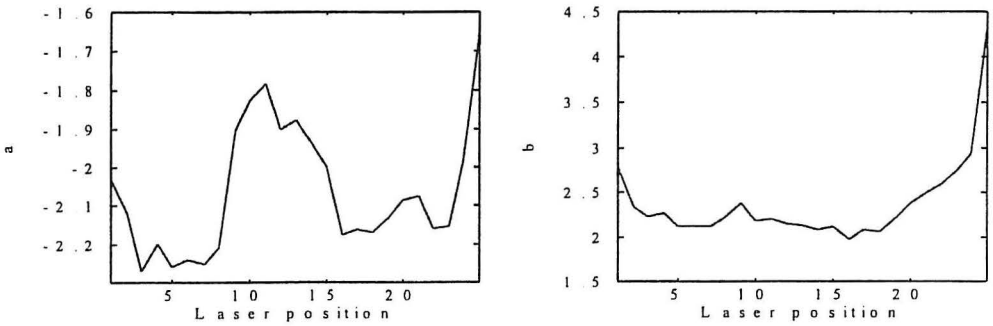

Figure 2.8 *Change in parameters a and b shown as a function of laser position*

2.3 Presentation of the Measured Filtered Data

In order to investigate the surface roughness closer (wave lengths < 10 m) the measured data have been filtered using a 6'th order highpass digital elliptic filter with 0.5 decibels of ripple in the passband and a stopband 20 decibels down. Figure 2.9 and 2.10, respectively, show the measured road surface profile highpass filtered and the corresponding PSD. Again, it becomes obvious that also the filtered road irregularities can be approximated sufficiently by a straight line in this double-logarithmic scale. However, it is seen that the slop *a* for the filtered road profiles is smaller than for the unfiltered road profiles. By considering figure 2.9 some more pronounced irregularities can be seen in the right side of the road at positions around 75 m and 125, respectively. These could be bumps/expansion joints at the approaches to the bridge.

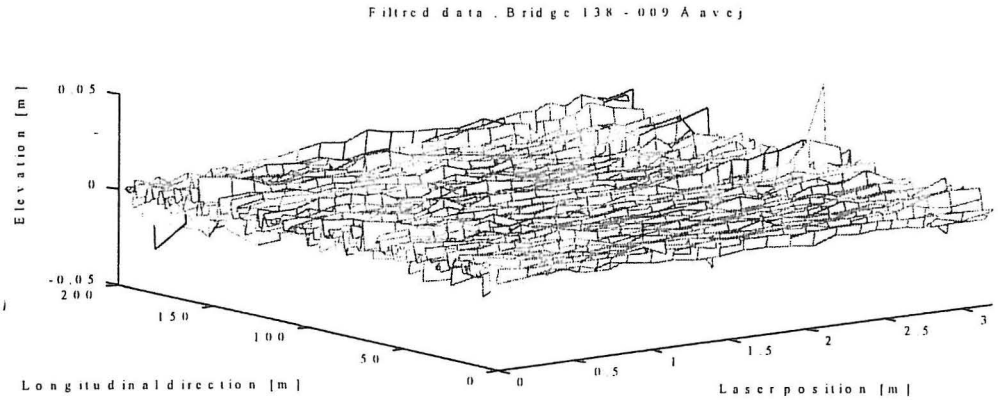

Figure 2.9 *The highpass filtered road profile from bridge 138 -009 (Åsvej). Laser no 1 in left side of the road, laser no. 25 in the right side of the road.*

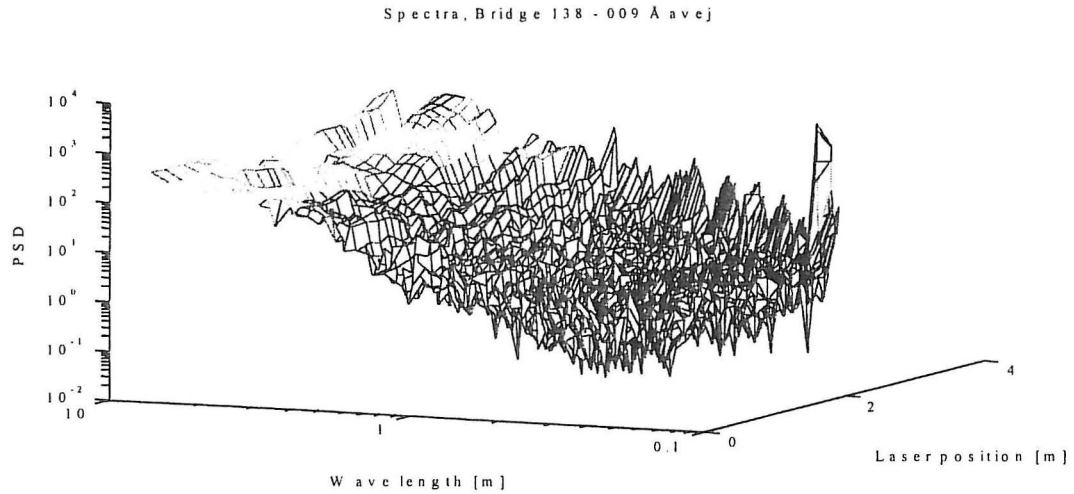

Figure 2.10 *PSD of the filtered road profile from bridge 138 -009 (Åsvej). Laser no 1 in left side of the road, laser no. 25 in the right side of the road.*

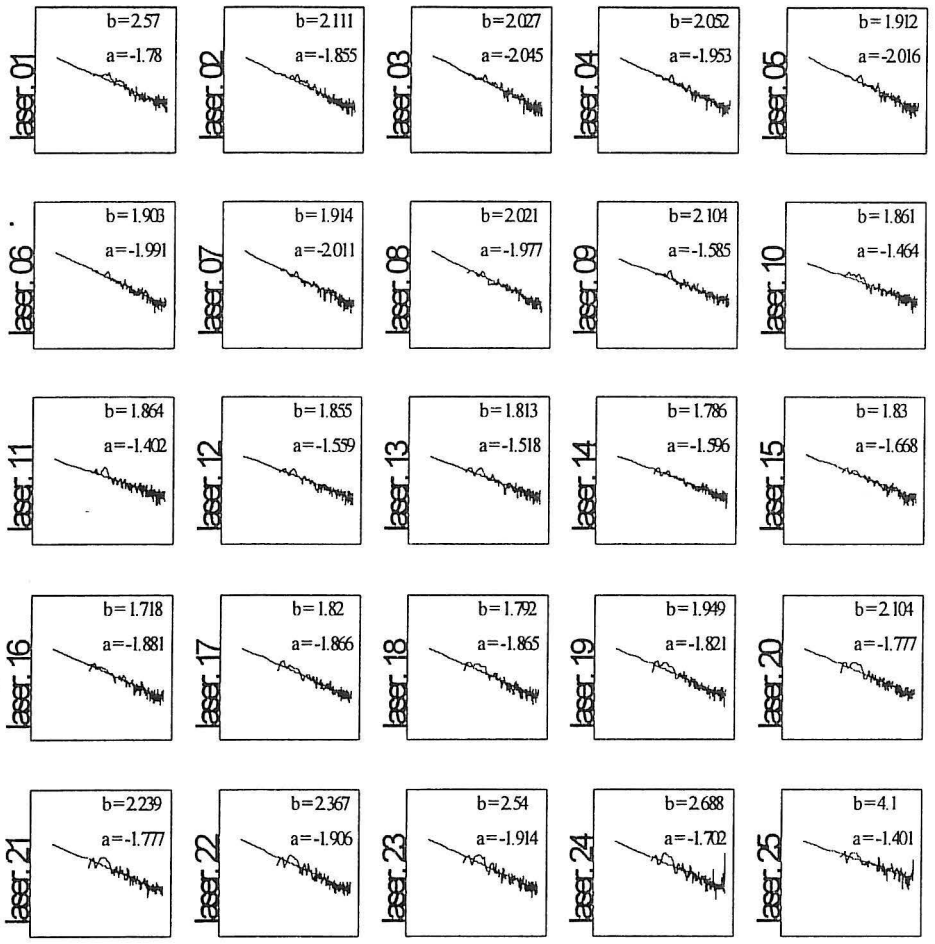

Figure 2.11 *PSD* $s_Y(k)$ *of the filtered road profile from bridge 138 -009 (Åsvej) shown for each laser position and wave number in a double logarithmic mapping together with a linear regression line given by equation (1).*

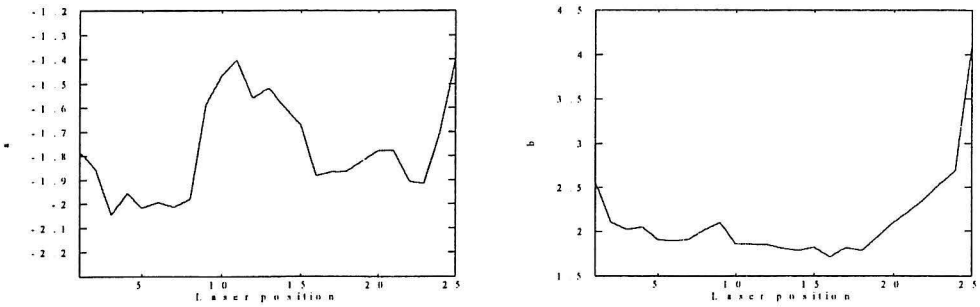

Figure 2.12 *Change in parameters a and b shown as a function of laser position*

Figure 2.11 shows the results obtained by the linear regression line using equation (1) to the PSD for each laser and figure 2.12 shows the variation in the parameters a and b. A comparison of these two figures with the corresponding figures 2.7 and 2.8 for the unfiltered road profiles does not show any significant differences.

In order to invesigate the correlation in transversal direction (x_2) between the time series measured with the 25 lasers the sample correlation coefficient function $\rho_{ZZ}(x_2^{(i)},x_2^{(j)})$ at the points $x_2^{(i)}$ and $x_2^{(j)}$ of lasers i and j is estimated by

$$\rho_{ZZ}(x_2^{(i)},x_2^{(i)}+x_2^{(j)}) = \frac{1}{N_1}\sum_{n=1}^{N_1} z(x_2^{(i)}+x_2^{(j)},x_2^{(n)})z(x_2^{(i)},x_2^{(n)})) \qquad (2)$$

where Z is the filtered road profile and N_1 is the number of data in a time series. The estimated correlation coefficient functions for transversal as well as longitudinal directions are shown in figures 2.13a and 2.13b, respectively. Eq(2) has also been used to estimate the correlation coefficient functions at points $x_2^{(i)}$ and $x_2^{(j)}$ laying on a line with an angle of 45 degrees, see figure 2.13c. The mean values of the correlation coefficient functions for the three directions are shown in figure 2.13d. Based on a visual comparison figure 2.13d indicates that the filtered road profile has a correlation coefficient function which depends only on the horizontal distance between points. The surface is then said to have properties which are covariance homogeneous and isotropic.

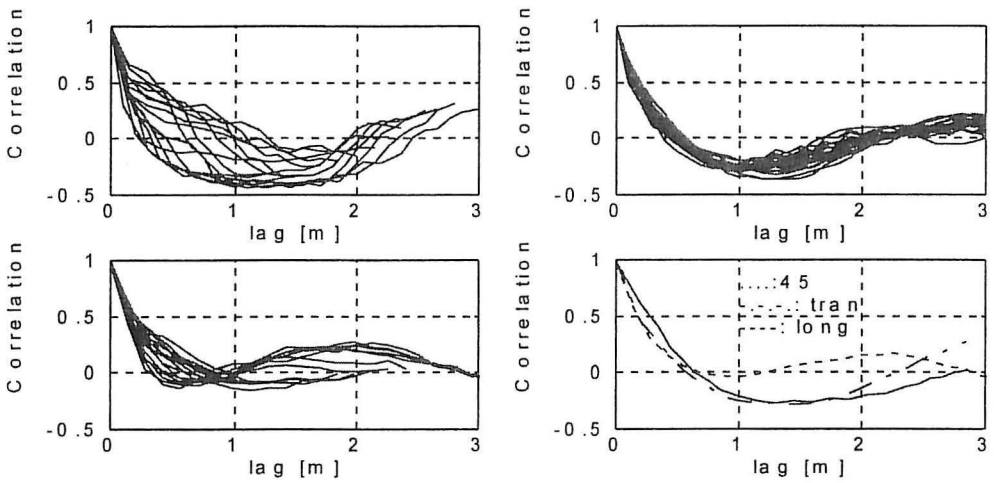

Figure 2.13 *The correlation coefficient functions in a) transversal direction, b)longitudinal direction, c) 45° direction and d) the mean values of the correlation coefficient functions for the three directions.*

3. STOCHASTIC MODEL OF SURFACE IRREGULARITIES

The aim of the following chapter is to establish a stochastic model for the surface irregularities. This model will model, based on the observations from figures 2.3.-2.13, the deterministic trends in transversal (wheel tracking) as well as longitudinal direction (some long-waved tendency) . Further, the bumps/expansion joints at the approaches to the bridge and the stochastic nature of the surface roughness will be included into the model. The stochastic model presented is based on a (x_1,x_2,x_3)-coordinate system see figure 3.1 placed on a horizontal smooth base surface of the road. The x_1 - axis is directed along the longitudinal and the x_2 - axis along the transversal direction. The origo is placed at one side of the road, so $(x_1,x_2) \in]-\infty, \infty[\times [0, B]$. B indicates the width of the road.

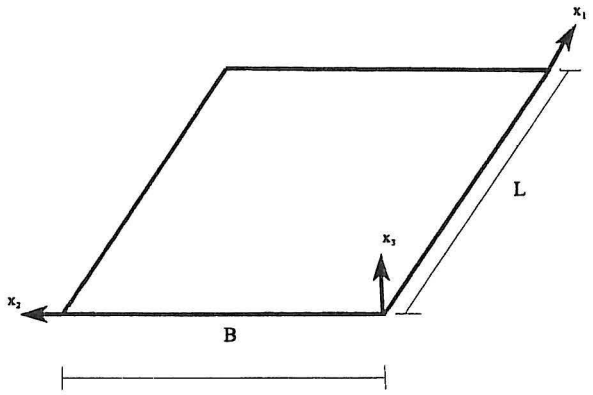

Figure 3.1 Geometry for stochastic model

The surface irregularities from the base line are modelled by the stochastic process $\{Z(x_1,x_2) \in [0, L] \times [0, B]\}$. This quantity is measured at N_2 discrete positions in the transverse direction equal to the number of lasers. In x_1 -direction the measurement points are sampled with the distance $\Delta x_1 = \frac{L}{N_1}$ where L is the measurement length and N_1 is the number of samples.

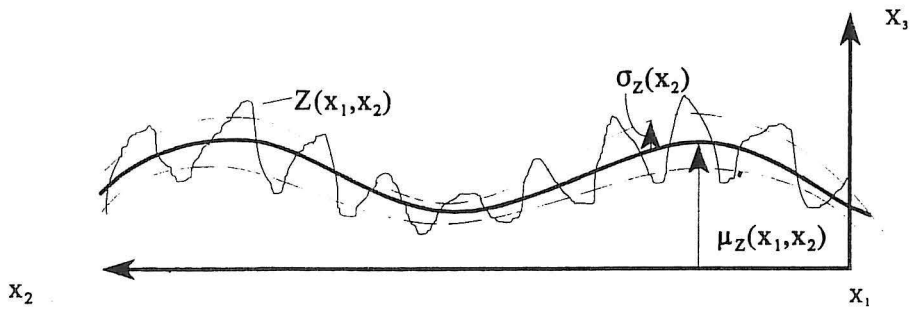

Figure 3.2 *Graphical interpretation of* $\mu_Z(x_1,x_2)$ *and* $\sigma_Z(x_2)$

For $Z(x_1, x_2)$ the following model is applied

$$Z(x_1,x_2) = \mu_Z(x_1,x_2) + \sigma_Z(x_2)Y(x_1,x_2) \tag{3}$$

$\mu_Z(x_1,x_2) = E[Z(x_1, x_2)]$ signifies the mean value function specifying the deterministic trends in the surface irregularities due to small hills or other low frequency trends in the longitudinal direction, expansion joints at the abutments of the bridge and wheel tracking in the transverse direction. The standard deviation $\sigma_Z(x_2) = (E[(Z(x_1, x_2) - \mu_Z(x_1,x_2))^2])^{1/2}$ is a measure of the magnitude of the surface irregularities on the top of the deterministic trends. This quantity is assumed to be homogeneous in the longitudinal direction, i.e. corresponding to no x_1- depending. The variation is believed to be larger at the "hills" than in the "valleys" due to polishing from traffic as sketched in figure 3.2. Finally, $\{Y(x_1,x_2) \in [0, L] \times [0, B]\}$ is a zero mean homogeneous isotropic Gaussian stochastic process with variance $\sigma^2_Y(x_1, x_2) \equiv 1$. The extend of low frequency trends and wheel tracking cannot be foreseen in advance. Hence $\mu_Z(x_1,x_2)$ and $\sigma_Z(x_2)$ should be considered as random variables generated by a number of basic variables entering the models of these quantities, which will be specified below. The indicated expectation for $\mu_Z(x_1,x_2)$ and $\sigma_Z(x_2)$ should then be interpreted as conditioned on these basic variables.

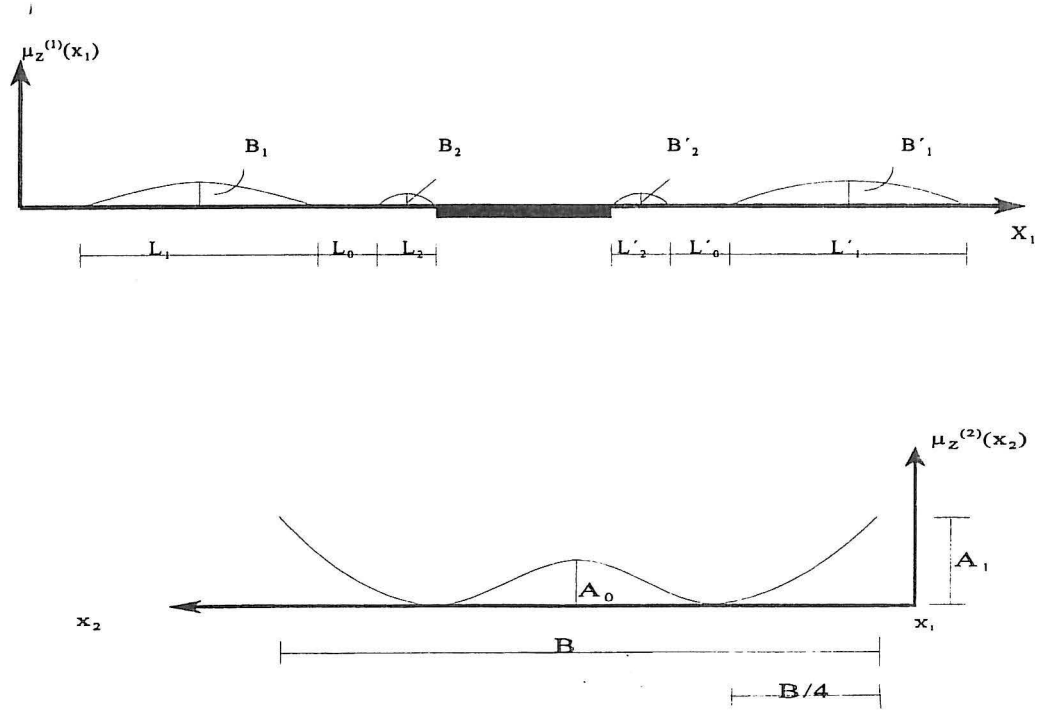

Figure 3.3 Model of mean-value function $\mu_Z(x_1,x_2) = \mu_Z^{(1)}(x_1,) + \mu_Z^{(2)}(x_2)$

The mean value function of the road surface is modelled as a sum of independent deterministic trends in the x_1 and x_2 direction, i.e. $\mu_Z(x_1,x_2) = \mu_Z^{(1)}(x_1,) + \mu_Z^{(2)}(x_2)$. The deterministic trend in the x_1 - direction has been selected in figure 3.3a. Half-sine irregularities of amplitude B_1, B_2, B_1' and B_2' and the wave-length terms L_1, L_2, L_1' and L_2' are present on the approaches to the bridge. The distances between the irregularities are denoted L_0 and L_0', respectively. The irregularities with amplitudes B_2 and B_2' are modelling the expansion joints whereas the irregularities with amplitudes B_1 and B_1' are supposed to represent some long-waved tendency in the longitudinal road profile, i.e. $L_1, L_1' >> L_2, L_2'$. The basic variables L_0, L_1, L_2, B_1, B_2, L_0', L_1', L_2', B_1', B_2' are assumed to be mutually independent variables. L_0 and L_0' are identically Rayleigh-distributed, $L_0,L_0' \sim R(\sigma^2_{L_0})$. Similarly, $B_1,B_1' \sim R(\sigma^2_{B_1})$, $B_2,B_2' \sim R(\sigma^2_{B_2})$, $L_1,L_1' \sim R(\sigma^2_{L_1})$, $L_2,L_2' \sim R(\sigma^2_{L_2})$ are supposed to be pairwise identically distributed stochastic variables.

The model for $\mu_Z(x_2)$ has been sketched in figure 3.3b. Only the wheel-tracking in one lane is shown. $\mu_Z(x_2)$ is assumed to be symmetric around $x_2 = B/2$. The profile is defined by the heights A_0 and A_1 , assuming a cubic spline between the node-points. Further, it is assumed that the term A_0 is deterministically related to A_1 according to

$$A_0 = \alpha_0 A_1 , \quad \alpha_0 \in [0,1] \tag{4}$$

$A_1 \sim R(\sigma^2_{A_1})$ is a Rayleigh-distributed random variable independent of the random variables generating the longitudinal profile $\mu_Z(x_1)$. The parameter α_0 is a deterministic decreasing function with age and traffic amount

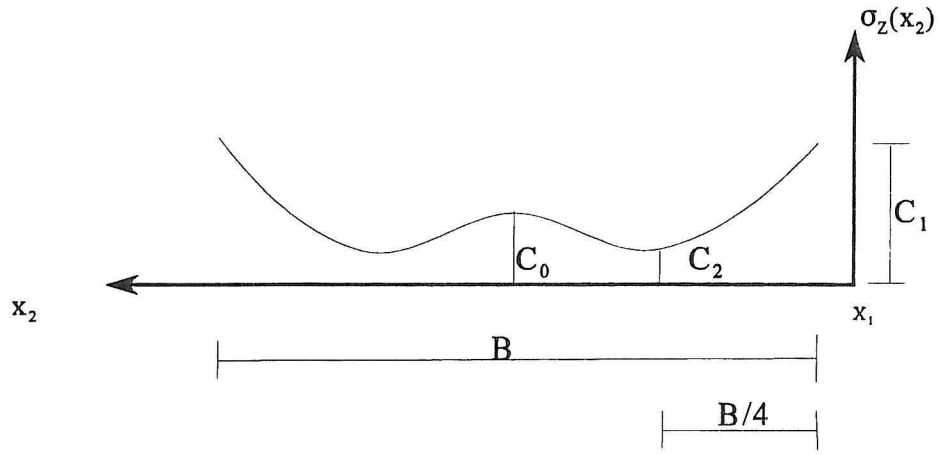

Figure 3.4 Model of standard deviation $\sigma_Z(x_2)$

The standard deviation in the transverse direction is modelled as shown in figure 3.4. Only one lane is shown and $\sigma_Z(x_2)$ *is* assumed to be symmetric around $x_2 = B/2$ as was the case for $\mu_Z(x_2)$. C_1 is assumed to represent the surface irregularities of the new laid road which is assumed to be

Rayleigh-distributed $C_1 \sim R(\sigma_{C_1}^2)$, and is assumed to be independent of the basic random variables generating $\mu_Z(x_1,x_2)$. C_0 and C_2 are reduced surface irregularities due to polishing. These are modelled as follows

$$\begin{aligned} C_0 &= \gamma_0 C_1 \qquad \gamma_0 \in [0,1] \\ C_2 &= \gamma_2 C_1 \qquad \gamma_2 \in [0,1] \end{aligned} \tag{5}$$

γ_0 and γ_2 are assumed to be deterministic decreasing functions of the ageing of the pavement and the traffic amount. Initially, samples of $\mu_Z(x_1,x_2)$ and $\sigma_Z(x_1,x_2)$ are generated upon generating independent samples of the quantities entering the models of these quantities. Assuming a realization $y(x_1,x_2)$ of the field $\{Y(x_1,x_2)\}$ is available, realizations of the road surface then become $Z(x_1,x_2) = \mu_Z(x_1,x_2) + \sigma_Z(x_1,x_2)\, y(x_1,x_2)$, cf. (3).

In order to calculate realizations of the stochastic field $\{Y(x_1,x_2) \in [0, L] \times [0, B]\}$ the following stochastic model is applied

$$Y(x_1,x_2) = \sum_{m=1}^{N_1} \sum_{n=1}^{N_2} A_{mn} \cos\left[2\pi\left(m\frac{x_1}{L} + n\frac{x_2}{B}\right) - \Phi_{mn}\right] + B_{mn} \cos\left[2\pi\left(m\frac{x_1}{L} - n\frac{x_2}{B}\right) - \Psi_{mn}\right] \tag{6}$$

In (6) $A_{mn} \sim R(\sigma_{A_{mn}}^2)$ and $B_{mn} \sim R(\sigma_{B_{mn}}^2)$ are Rayleigh distributed random variables with the parameters $\sigma_{A_{mn}}^2$ and $\sigma_{B_{mn}}^2$, and $\Phi_{mn} \sim U(0,2\pi)$, $\Psi_{mn} \sim U(0,2\pi)$ are uniformly distributed over the interval $[0, 2\pi]$. All the random variables A_{mn}, B_{mn}, and Φ_{mn}, Ψ_{mn} in (6) are mutually independent. If $A \sim R(\sigma^2)$ and $\Phi \sim U(0,2\pi)$ it is well-known that $X = A\cos(x - \Phi)$ becomes normal distributed with zero mean and variance σ^2, i.e $X \sim N(0, \sigma^2)$. Hence, (6) consists of a sum of mutually independent zero mean independent normal variables. $\{Y(x_1,x_2)\}$ is then a zero mean Gaussian process from the various mixing theorems generalizing the central limit theorem to stochastic processes. The auto-covariance function of (6) becomes

$$\kappa_{YY}(\xi_1,\xi_2) = E[Y(x_1,x_2)Y(x_1+\xi_1,x_2+\xi_2)] \approx \sum_{m=1}^{N_1}\sum_{n=1}^{N_2}\left[\sigma_{A_{mn}}^2 \cos\left(2\pi(m\frac{\xi_1}{L} + n\frac{\xi_2}{B})\right) + \sigma_{B_{mn}}^2 \cos\left(2\pi(m\frac{\xi_1}{L} - n\frac{\xi_2}{B})\right)\right] \tag{7}$$

The straight forward insertion of (6) into the left -hand side of (7) results in a four-double sum. However, only the diagonal terms in this four-double sum retains, using the mutual independence of the involved stochastic variables. Further reduction has been done using the following results for $A \sim R(\sigma^2)$ and $\Phi \sim U(0,2\pi)$.

$$E[A^2] = \int_0^\infty a^2 \frac{a}{\sigma^2} \exp\left(-\frac{a^2}{2\sigma^2}\right) da = 2\sigma^2 \tag{8}$$

$$E[\cos(x + \Phi)\cos(y + \Phi)] = \int_0^{2\pi} \cos(x + u)\cos(y + u)\frac{1}{2\pi}du = \frac{1}{2}\cos(x - y) \qquad (9)$$

The homogeneity of $\{Y(x_1,x_2)\}$ follows from the last statement of (7). Apparently, $\kappa_{YY}(\xi_1,\xi_2)$ fulfills the symmetry property

$$\kappa_{YY}(\xi_1,\xi_2) = \kappa_{YY}(-\xi_1,-\xi_2) \qquad (10)$$

The following 2-dimensional Fourier transformation applies

$$\left.\begin{aligned} \kappa_{YY}(\xi_1,\xi_2) &= \int_{-\infty}^{\infty}\int_{-\infty}^{\infty} e^{i(\xi_1 k_1 + \xi_2 k_2)} S_{YY}(k_1,k_2)dk_1 dk_2 \\ S_{YY}(k_1,k_2) &= \frac{1}{4\pi^2}\int_{-\infty}^{\infty}\int_{-\infty}^{\infty} e^{-i(\xi_1 k_1 + \xi_2 k_2)} \kappa_{YY}(\xi_1,\xi_2)d\xi_1 d\xi_2 \end{aligned}\right\} \qquad (11)$$

(11) is known as the so-called Wiener - Khintchine relations. $S_{YY}(k_1,k_2)$ is termed the auto-spectral density of the surface irregularities process $\{Y(x_1,x_2)\}$. From (10) and the 2nd part of (11) follow the symmetry properties

$$\left.\begin{aligned} S_{YY}(k_1,k_2) &= S_{YY}(-k_1,-k_2) \\ S_{YY}(k_1,k_2) &= S^{*}_{YY}(-k_1,-k_2) \end{aligned}\right\} \qquad (12)$$

where * signifies complex conjugation. From (12) it is concluded that $S_{YY}(k_1,k_2)$ is real and symmetric in the sense of the first part of (12). Since, both $S_{YY}(k_1,k_2)$ and $\kappa_{YY}(\xi_1,\xi_2)$ are real, the imaginary parts of $e^{\pm i(\xi_1 k_1 + \xi_2 k_2)}$ cancel, and may be replaced by $\cos(\xi_1 k_1 + \xi_2 k_2)$. The first part of (12) can then be written

$$\kappa_{YY}(\xi_1,\xi_2) = \int_{-\infty}^{\infty}\int_{-\infty}^{\infty}\cos(k_1\xi_1+k_2\xi_2)S_{YY}(k_1,k_2)dx_1dx_2 =$$

$$\int_0^{\infty}\int_0^{\infty}\left[2\cos(k_1\xi_1)\cos(k_2\xi_2)\Big(S_{YY}(k_1,k_2)+S_{YY}(-k_1,k_2)\Big)dk_1dk_2 -\right.$$

$$\left.2\sin(k_1\xi_1)\sin(k_2\xi_2)\Big(S_{YY}(k_1,k_2)-S_{YY}(-k_1,k_2)\Big)dk_1dk_2\right] \approx \qquad (13)$$

$$\sum_{m=1}^{N_1}\sum_{n=1}^{N_2}\left[2\cos\Big(2\pi m\frac{\xi_1}{L}\Big)\cos\Big(2\pi n\frac{\xi_2}{B}\Big)\Big(S_{YY}(m\Delta k_1,n\Delta k_2)+S_{YY}(-m\Delta k_1,n\Delta k_2)\Big)\Delta k_1\Delta k_2 -\right.$$

$$\left.2\sin\Big(2\pi m\frac{\xi_1}{L}\Big)\sin\Big(2\pi n\frac{\xi_2}{B}\Big)\Big(S_{YY}(m\Delta k_1,n\Delta k_2)-S_{YY}(-m\Delta k_1,n\Delta k_2)\Big)\Delta k_1\Delta k_2\right]$$

where

$$\Delta k_1 = \frac{2\pi}{L} \quad , \quad \Delta k_2 = \frac{2\pi}{B} \qquad (14)$$

Upon comparison (7) and (13) the following expressions are obtained for the parameters $\sigma^2_{A_{mn}}$ and $\sigma^2_{B_{mn}}$

$$\left.\begin{aligned}\sigma^2_{A_{mn}} &= 2S_{YY}(m\Delta k_1,n\Delta k_2)\Delta k_1\Delta k_2 \quad , \quad m=1,\ldots,N_1\\ \sigma^2_{B_{mn}} &= 2S_{YY}(-m\Delta k_1,n\Delta k_2)\Delta k_1\Delta k_2 \quad , \quad n=1,\ldots,N_2\end{aligned}\right\} \qquad (15)$$

Assuming $S_{YY}(k_1,k_2)$ to be known, the application of (6) can now be explained in the following steps:

1) Initially, the parameters $\sigma^2_{A_{mn}}$ and $\sigma^2_{B_{mn}}$ are calculated from (15).

2) For all (m,n) generate independent samples of the Rayleigh distributed random variables $A_{mn} \sim R(\sigma^2_{A_{mn}})$ and $B_{mn} \sim R(\sigma^2_{B_{mn}})$ as well as the mutually independent uniformly distributed variables $\Phi_{mn} \sim U(0,2\pi)$, $\Psi_{mn} \sim U(0,2\pi)$ by means of a random generator.

3) The corresponding realizations $y(x_1,x_2)$ of $\{Y(x_1,x_2)\}$ are calculated by (6).

Assuming a one-sided one-dimensional auto-spectrum $s_Y(k)$ of the surface irregularities, see section 2, is known and the field $\{Y(x_1,x_2)\}$ is assumed to be known, a relationship between $S_{YY}(k_1,k_2)$ and $s_Y(k)$ has to be established. The one-dimensional auto-covariance function for surface irregularities along the x_1 - axis for a fixed x_2 becomes

$$k_{YY}(\xi_1) = E[Y(x_1,x_2)Y(x_1+\xi_1,x_2)] = \kappa_{YY}(\xi_1,0) \tag{16}$$

Similar to (11) this function admits the mutual Fourier transforms

$$\left.\begin{aligned} k_{YY}(\xi) &= \int_{-\infty}^{\infty} e^{i\xi k} s_{YY}(k)dk \\ s_{YY}(k) &= \frac{1}{2\pi}\int_{-\infty}^{\infty} e^{-i\xi k} k_{YY}(\xi)d\xi \end{aligned}\right\} \tag{17}$$

$s_{YY}(k) = s_{YY}(-k) = s^*_{YY}(k)$ signifies the double-sided one-dimensional auto-spectrum. This is related to the two-dimensional auto-spectrum defined in (10) as follows

$$s_{YY}(k) = \int_{-\infty}^{\infty} S_{YY}(k,k_2)dk_2 \tag{18}$$

Due to the symmetry properties $k_{YY}(\xi) = k_{YY}(-\xi)$ and $s_{YY}(k) = s_{YY}(-k)$, (18) can be replaced by the mutual cosine-transforms

$$\left.\begin{aligned} k_{YY}(\xi) &= \int_0^{\infty} \cos(k\xi) s_Y(k)dk \\ s_Y(k) &= \frac{2}{\pi}\int_0^{\infty} \cos(k\xi) k_{YY}(\xi)d\xi \end{aligned}\right\} \tag{19}$$

$$s_Y(k) = 2s_{YY}(k) \quad , \quad k > 0 \tag{20}$$

$s_Y(k)$ is the spectrum shown in figure 2.7 . Instead of the (x_1,x_2) coordinate system an arbitrary rotated (x'_1,x'_2) system is considered, see figure 3.6.

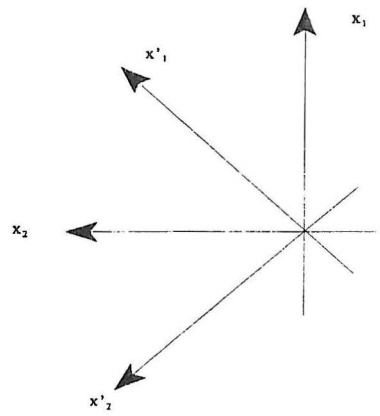

Figure 3.6 *Definition of rotated coordinate system*

Now, $S'_{YY}(k'_1,k'_2)$ signifies the auto-spectrum measured in the rotated coordinate system. If $S'_{YY}(k'_1,k'_2) = S_{YY}(k'_1,k'_2)$ the random Gaussian field is termed isotropic. In this case $S_{YY}(k_1,k_2)$ only depends on k_1 and k_2 via the magnitude $k = |k| = (k_1^2 + k_2^2)^{\frac{1}{2}}$ of the wave-number vector, i.e. $S_{YY}(k_1,k_2) = S_{YY}(k)$. Based on the analysis in section 2 such an assumption may be adopted for the present field. Similarly, the auto-covariance function $\kappa_{YY}(\xi_1,\xi_2)$ does only depend on the separation distance $\xi = |\xi|$ between the coordinate points, i.e. $\kappa_{YY}(\xi_1,\xi_2) = \kappa_{YY}(\xi)$. Upon evaluation the auto-spectrum in polar coordinates one has

$$
\begin{aligned}
S_{YY}(k) &= \frac{1}{4\pi^2}\int_0^{\infty}\int_0^{2\pi}\kappa_{YY}(\xi)e^{-ik\cdot\xi}\xi d\xi d\phi \\
&= \frac{1}{4\pi^2}\int_0^{\infty}\xi\kappa_{YY}(\xi)\int_0^{2\pi}\cos(k\xi\cos\phi)d\phi d\xi \\
&= \frac{1}{2\pi}\int_0^{\infty}\xi J_0(k\xi)k_{YY}(\xi)d\xi
\end{aligned}
\qquad (21)
$$

where ϕ is the angle between the vectors ξ and $\boldsymbol{k}$, and $J_0(x)$ is the Bessel function of zero order and 1st kind. $\kappa_{YY}(\xi)$ specifies the covariance between 2 points with the spacing ξ, and is in principle equal to the measured one-dimensional auto-covariance function $k_{YY}(\xi)$. Hence, (21) provides a relation between the two-dimensional auto-spectrum of an isotropic field and the one-dimensional auto-covariance function. (21) shows that $k_{YY}(\xi)$ and $2\pi\ S_{YY}(k)$ are mutual Hankel transforms. The inverse relation then reads

$$k_{YY}(\xi) = 2\pi \int_0^\infty k J_0(k\xi) S_{YY}(k) dk \tag{22}$$

Assume that $k_{YY}(\xi)$ can be written

$$\left.\begin{aligned} k_{YY}(\xi) &= \sum_{j=1}^{J} c_j e^{-d_j \xi} \cos(e_j \xi) \\ \sum_{j=1}^{J} c_j &= 1 \end{aligned}\right\} \tag{23}$$

where c_j, d_j and e_j are real constants. Then (21) becomes

$$S_{YY}(k) = \frac{1}{2\pi} Re\left(\sum_{j=1}^{J} c_j \frac{p_j}{(k^2 + p_j^2)^{3/2}} \right) , \quad p_j = d_j + ie_j \tag{24}$$

At the derivation of (24) the following version of the Lipschitz integral has been used , Watson (1966)

$$\begin{aligned} &\int_0^\infty \xi J_0(k\xi) e^{-d\xi} \cos(e\xi) d\xi = Re\left(\int_0^\infty \xi J_0(k\xi) e^{(-d+ie)\xi} d\xi \right) = \\ &Re\left(\sum_{j=1}^{J} c_j \frac{p_j}{(k^2 + p_j^2)^{3/2}} \right) \quad , \quad p_j = d_j + ie_j \end{aligned} \tag{25}$$

(24) is the expression for $S_{YY}(k_1, k_2)$ searched for.

3.1 Example

In the following example the proposed stochastic model for the surface irregularities will be used to calculate a realization $z(x_1,x_2)$ of the road surface.

First, the expression in eq. (23) is fitted to the mean of the three curves in figure 2.13d by using three terms. This calculation is performed using *constr.m* from the MATLAB Optimization Toolbox, Mathworks. Next a realization $y(x_1,x_2)$ of the field $\{Y(x_1,x_2)\}$ is calculated as described at page 16. A realization $y(x_1,x_2)$ of the field $\{Y(x_1,x_2)\}$ is then obtained from eq.(3) using the values of the basic varibles in table 3.1 and the models of the mean-value function and standard deviation given in figures 3.3 and 3.4, respectively.

Basic Variabel (X)	*Distribution*	*Standard Deviation (σ_X)*
Wave length (L_1)	Rayleigh	50.0 m
Wave length (L_2)	Rayleigh	0.50 m
Wave length (L_1')	Rayleigh	50.0 m
Wave length (L_2')	Rayleigh	0.50 m
Distance (L_0)	Rayleigh	10.0 m
Distance (L_0')	Rayleigh	10.0 m
Amplitude (B_1)	Rayleigh	0.01 m
Amplitude (B_2)	Rayleigh	0.002 m
Amplitude (B_1')	Rayleigh	0.01 m
Amplitude (B_2')	Rayleigh	0.002 m
Scale factor (α_0)	Deterministic	0.8
Scale factor (γ_0)	Deterministic	0.6
Scale factor (γ_2)	Deterministic	0.3
Profile height (A_1)	Deterministic	0.003 m
Irregularity height (C_1)	Deterministic	0.001 m

Table 3.1: Statistical characteristics of basic variables.

Figures 3.7, 3.8. and 3.9 show the estimated mean-value function, a realization of the stochastic field $\{Y(x_1,x_2)\}$ and a realization of the field $\{Z(x_1,x_2)\}$, respectively. Figure 3.10 shows the auto-spectra of the stochastic field $\{Y(x_1,x_2)\}$ obtained from a simulation and from measurement, respectively.

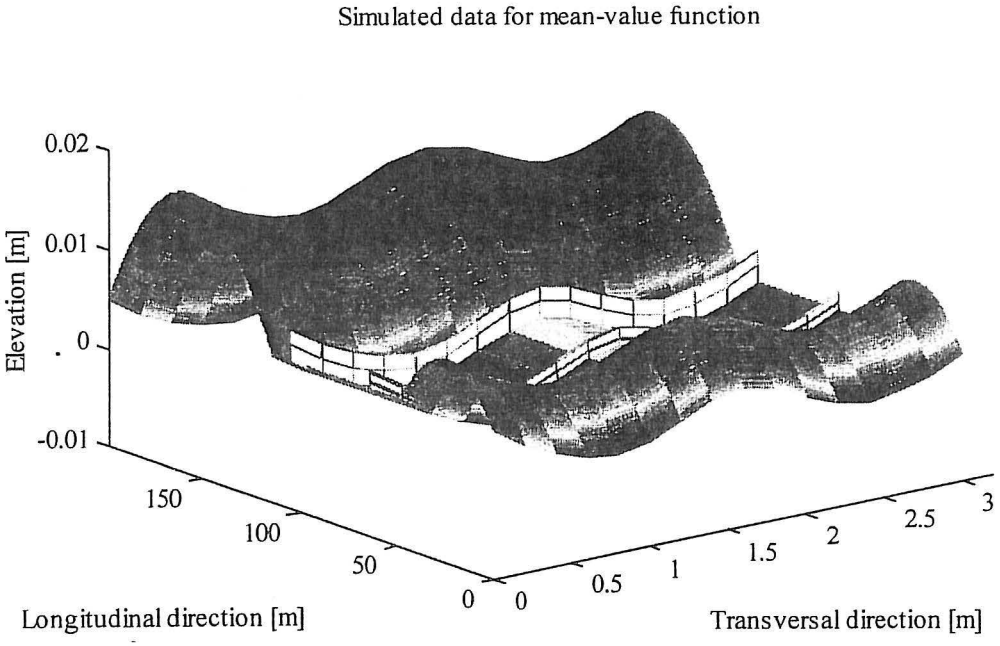

Figure 3.7 *A realization of the mean-value function* $\mu(x_1,x_2)$.

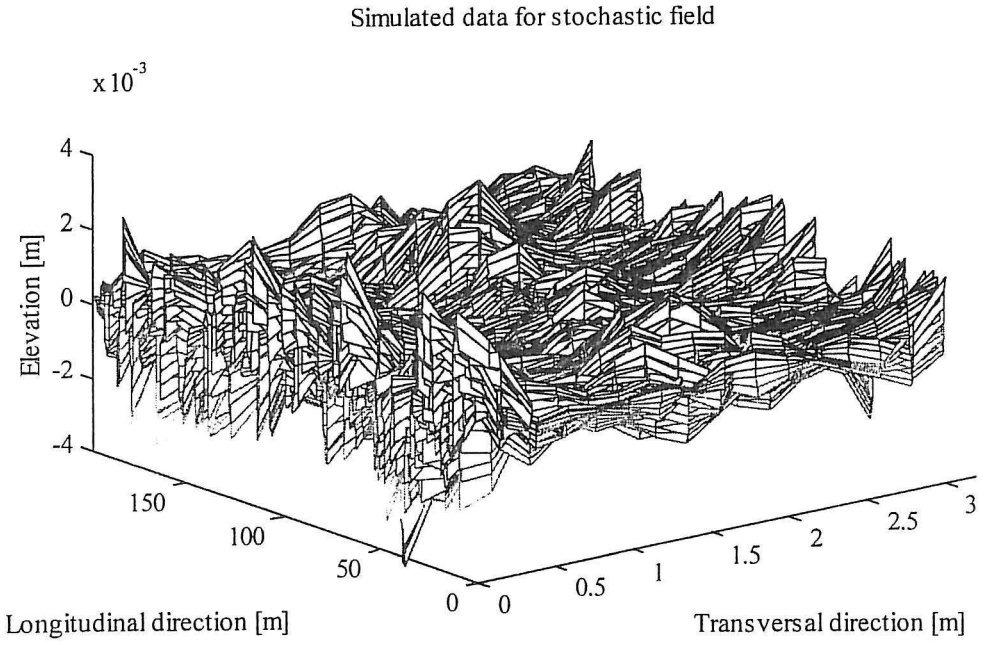

Figure 3.8 *A realization of the stochastic field* $\{Y(x_1,x_2)\}$.

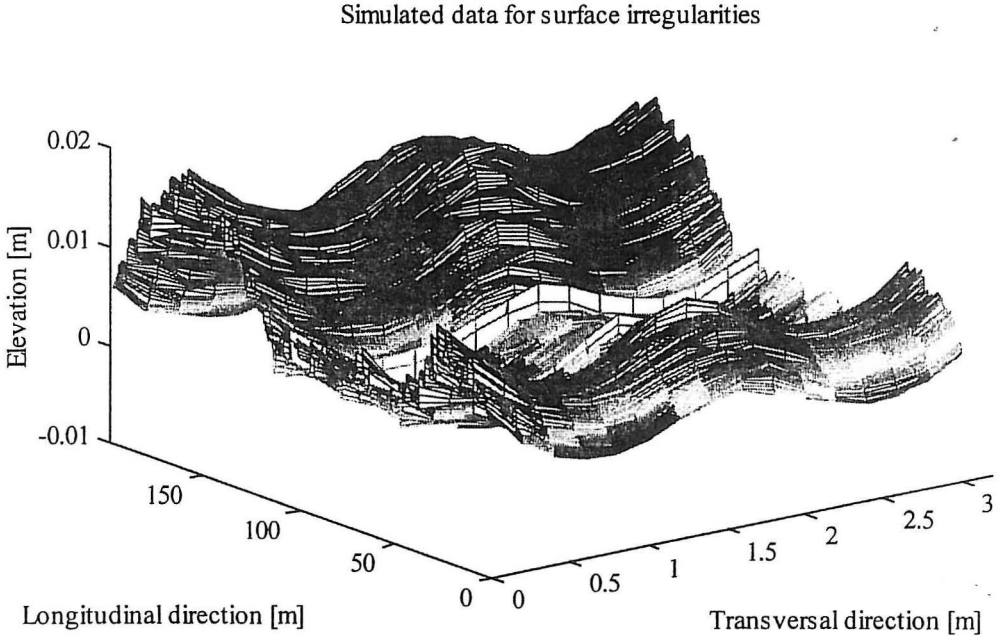

Figure 3.9 *A realization of the field* $\{Z(x_1,x_2)\}$

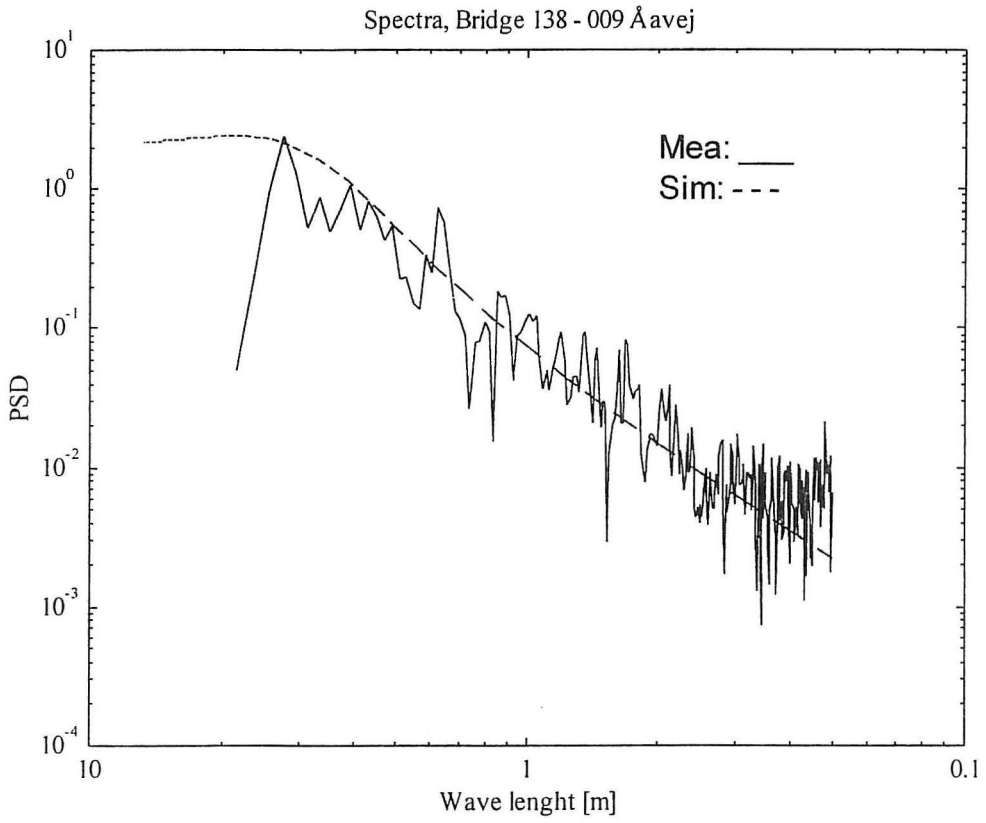

Figure 3.10 *PSD of the filtered road profile (only one channel) and a simulated realization of* the stochastic field $\{Y(x_1,x_2)\}$, respectively, *shown as function wave number in a double logarithmic mapping.*

4. CONCLUSION

The present paper establishes a two-dimensional spectral description of the road roughness surface based on measurements from a Danish road using a so-called Profilograph. The stochastic model for the surface irregularities models, based on the observations from the measured data, the deterministic trends in transversal (wheel tracking) as well as longitudinal direction (some long-waved tendency). Further, the bumps/expansion joints at the approaches to the bridge and the stochastic nature of the surface rougness are included into the model.

5. ACKNOWLEDGEMENT

The present research was partially supported by The Danish Technical Research Council within the project: *Dynamic amplification factor of vehicle loadings on smaller bridges.*

6. REFERENCES

Dodds, C.J., & Robson, J.D. *The description of Road Surface Roughness.* Journal of Sound and Vibration, Vol. 31, No. 2, pp. 175-183, 1973.

Green, M.F. & Cebon, D. *Dynamic Response of Highway Bridges to Heavy Vehicle Loads: Theory and Experimental Validation.* Journal of Sound & Vibration ,Vol. 170, No. 1, pp. 51-78, 1994.

Honda, H. Kajikawa, Y., Kobori, T. *Spectra of Road Surfaces Roughness on Bridges.* ASCE, Vol. 108, No. ST9, pp. 1956-1966, 1982.

Inbanathan, M.J., Wieland, M. *Bridge Vibrations due to Vehicle Moving over Rough Surface.* Journal of Structural Engineering. ASCE, Vol. 113, No. 9, pp. 1994-2008, 1987.

Kirkegaard, P.H., Nielsen, S.R.K, & Enevoldsen, I *Vehicle - Bridge Dynamics, A literature Review*, Aalborg University, 1997.

Marcondes, J., Burgess, G.J., Harichandran, R. *Spectral Analysis of Highway Pavement Rougness.* Journal of Transportation Engineering, Vol. 117, No. 5, 1991.

Mathieu, H., Calgaro, J.A. & Prat, M. *Concerning Development of Models of Traffic Loading and Rules for the Specification of Bridge Loads.* Final Report to the Commission of the European Communities on Contract No. PR2/90/7750/RN/46, 1991.

Paultre, P., Chaallal, O. & Proulx, J. *Bridge Dynamics and Dynamic Amplification Factors - Review of Analytical and Experimental Findings.* Canada Journal of Civil Engineering, Vol. 19, No. 2, pp. 260-278, 1992.

Schmidt, B. & Taudorf, A. *Experiences in using Profilograph, A laser-Based Equipment for Profilmetric Measurements of Pavement Surface,*. 1996.

Watson, G.N. *A Treatise of the Theory on Bessel Functions.* Cambridge at the University Press, 1966.

STRUCTURAL RELIABILITY THEORY SERIES

PAPER NO 141: H. U. Köylüoğlu, S. R. K. Nielsen & A. Ş. Çakmak: *Uncertain Buckling Load and Reliability of Columns with Uncertain Properties.* ISSN 0902-7513 R9524.

PAPER NO. 142: S. R. K. Nielsen & R. Iwankiewicz: *Response of Non-Linear Systems to Renewal Impulses by Path Integration.* ISSN 0902-7513 R9512.

PAPER NO. 143: H. U. Köylüoğlu, A. Ş. Çakmak & S. R. K. Nielsen: *Midbroken Reinforced Concrete Shear Frames Due to Earthquakes. - A Hysteretic Model to Quantify Damage at the Storey Level.* ISSN 1395-7953 R9630.

PAPER NO. 144: S. Engelund: *Probabilistic Models and Computational Methods for Chloride Ingress in Concrete.* Ph.D.-Thesis. ISSN 1395-7953 R9707.

PAPER NO. 145: H. U. Köylüoğlu, S. R. K. Nielsen, Jamison Abbott & A. Ş. Çakmak: *Local and Modal Damage Indicators for Reinforced Concrete Shear Frames subject to Earthquakes.* ISSN 0902-7513 R9521

PAPER NO. 146: P. H. Kirkegaard, S. R. K. Nielsen, R. C. Micaletti & A. Ş. Çakmak: *Identification of a Maximum Softening Damage Indicator of RC-Structures using Time-Frequency Techniques.* ISSN 0902-7513 R9522.

PAPER NO. 147: R. C. Micaletti, A. Ş. Çakmak, S. R. K. Nielsen & P. H. Kirkegaard: *Construction of Time-Dependent Spectra using Wavelet Analysis for Determination of Global Damage.* ISSN 0902-7513 R9517.

PAPER NO. 148: H. U. Köylüoğlu, S. R. K. Nielsen & A. Ş. Çakmak: *Hysteretic MDOF Model to Quantify Damage for TC Shear Frames subject to Earthquakes.* ISSN 1395-7953 R9601.

PAPER NO. 149: P. S. Skjærbæk, S. R. K. Nielsen & A. Ş. Çakmak: *Damage Location of Severely Damaged RC-Structures based on Measured Eigenperiods from a Single Response.* ISSN 0902-7513 R9518.

PAPER NO. 150: S. R. K. Nielsen & H. U. Köylüoğlu: *Path Integration applied to Structural Systems with Uncertain Properties.* ISSN 1395-7953 R9602.

PAPER NO. 151: H. U. Köylüoğlu & S. R. K. Nielsen: *System Dynamics and Modified Cumulant Neglect Closure Schemes.* ISSN 1395-7953 R9603.

PAPER NO. 152: R. C. Micaletti, A. Ş. Çakmak, S. R. K. Nielsen, H. U. Köylüoğlu: *Approximate Analytical Solution for the 2nd-Order moments of a SDOF Hysteretic Oscillator with Low Yield Levels Excited by Stationary Gaussian White Noise.* ISSN 1395-7953 R9715.

PAPER NO. 153: R. C. Micaletti, A. Ş. Çakmak, S. R. K. Nielsen & H. U. Köylüoğlu: *A Solution Method for Linear and Geometrically Nonlinear MDOF Systems with Random Properties subject to Random Excitation.* ISSN 1395-7953 R9632.

PAPER NO. 154: J. D. Sørensen, M. H. Faber, I. B. Kroon: *Optimal Reliability-Based Planning of Experiments for POD Curves.* ISSN 1395-7953 R9542.

STRUCTURAL RELIABILITY THEORY SERIES

PAPER NO. 155: J. D. Sørensen, S. Engelund: *Stochastic Finite Elements in Reliability-Based Structural Optimization.* ISSN 1395-7953 R9543.

PAPER NO. 156: C. Pedersen, P. Thoft-Christensen: *Guidelines for Interactive Reliability-Based Structural Optimization using Quasi-Newton Algorithms.* ISSN 1395-7953 R9615.

PAPER NO. 157: P. Thoft-Christensen, F. M. Jensen, C. R. Middleton, A. Blackmore: *Assessment of the Reliability of Concrete Slab Bridges.* ISSN 1395-7953 R9616.

PAPÈR NO. 158: P. Thoft-Christensen: *Re-Assessment of Concrete Bridges.* ISSN 1395-7953 R9605.

PAPER NO. 159: H. I. Hansen, P. Thoft-Christensen: *Wind Tunnel Testing of Active Control System for Bridges.* ISSN 1395-7953 R9662.

PAPER NO 160: C. Pedersen: *Interactive Reliability-Based Optimization of Structural Systems.* Ph.D.-Thesis. ISSN 1395-7953 R9638.

PAPER NO. 161: S. Engelund, J. D. Sørensen: *Stochastic Models for Chloride-initiated Corrosion in Reinforced Concrete.*ISSN 1395-7953 R9608.

PAPER NO. 164: P. Thoft-Christensen: *Bridge Management Systems. Present and Future.* ISSN 1395-7953 R9711.

PAPER NO. 165: P. H. Kirkegaard, F. M. Jensen, P. Thoft-Christensen: *Modelling of Surface Ships using Artificial Neural Networks.* ISSN 1593-7953 R9625.

PAPER NO. 166: S. R. K. Nielsen, S. Krenk: *Stochastic Response of Energy Balanced Model for Wortex-Induced Vibration.* ISSN 1395-7953 R9710.

PAPER NO. 167: S.R.K. Nielsen, R. Iwankiewicz: *Dynamic systems Driven by Non-Poissonian Impulses: Markov Vector Approach.* ISSN 1395-7953 R9705.

PAPER NO. 168: P. Thoft-Christensen: *Lifetime Reliability Assessment of Concrete Slab Bridges.* ISSN 1395-7953 R9717.

PAPER NO. 169: P. H. Kirkegaard, S. R. K. Nielsen, I. Enevoldsen: *Heavy Vehicles on Minor Highway Bridges - A Literature Review.* ISSN 1395-7953 R9719.

PAPER NO. 170: S.R.K. Nielsen, P.H. Kirkegaard, I. Enevoldsen: *Heavy Vehicles on Minor Highway Bridges - Stochastic Modelling of Surface Irregularities.* ISSN 1395-7953 R9720.

PAPER NO. 171: P. H. Kirkegaard, S. R. K. Nielsen, I. Enevoldsen: *Heavy Vehicles on Minor Highway Bridges - Dynamic Modelling of Vehicles and Bridges.* ISSN 1395-7953 R9721.

PAPER NO. 172: P. H. Kirkegaard, S. R. K. Nielsen, I. Enevoldsen: *Heavy Vehicles on Minor Highway Bridges - Calculation of Dynamic Impact Factors from Selected Crossing Scenarios.* ISSN 1395-7953 R9722.

Department of Building Technology and Structural Engineering
Aalborg University, Sohngaardsholmsvej 57, DK 9000 Aalborg
Telephone: +45 9635 8080 Telefax: +45 9814 8243